The Astrophysical Journal Letters, 724:L113–L117, 2010 November 20 doi:10.1088/2041-8205/724/1/L113

MAGNETIC FIELD STRUCTURE IN A HIGH-MASS OUTFLOW/DISK SYSTEM

H. Beuther[1], W. H. T. Vlemmings[2], R. Rao[3,4], and F. F. S. van der Tak[5]
[1] Max-Planck-Institute for Astronomy, Königstuhl 17, 69117 Heidelberg, Germany; beuther@mpia.de
[2] Argelander Institute for Astronomy, University of Bonn, Auf dem Hügel 71, 53121 Bonn, Germany; wouter@astro.uni-bonn.de
[3] Academia Sinica, Institute of Astronomy and Astrophysics, Taipei, Taiwan
[4] Submillimeter Array, 645 N. Aohoku Pl, Hilo, HI 96720, USA; rrao@sma.hawaii.edu
[5] SRON Netherlands Institute for Space Research, Landleven 12, 9747 AD Groningen, The Netherlands; vdtak@sron.nl
Received 2010 May 20; accepted 2010 October 7; published 2010 November 3

ABSTRACT

To characterize the magnetic field structure of the outflow and core region within a prototypical high-mass star-forming region, we analyzed polarized CO(3–2)—for the first time observed with the Submillimeter Array—as well as 880 μm submillimeter continuum emission from the high-mass outflow/disk system IRAS 18089−1732. Both emission features with polarization degrees at a few percent level indicate that the magnetic field structure is largely aligned with the outflow/jet orientation from small core scales to larger outflow scales. Although quantitative estimates are crude, the analysis indicates that turbulent energy dominates over magnetic energy. The data also suggest a magnetic field strength increase from the lower-density envelope to the higher-density core.

Key words: ISM: jets and outflows – stars: early-type – stars: formation – stars: individual (IRAS 18089−1732) – techniques: polarimetric – techniques: spectroscopic

Online-only material: machine-readable table

1. INTRODUCTION

The influence of magnetic fields on star formation processes has been intensely discussed for decades (e.g., Crutcher 2005). For magnetically supported molecular clouds, the magnetic field structure is expected to deform during cloud collapse, and theory predicts an hour-glass-shaped magnetic field structure pinched toward the protostar (e.g., Stahler & Palla 2005). This pinched magnetic field morphology is also required in the classical jet-launching scenario, where the gas is ejected from the accretion disk along the bent magnetic field lines (e.g., Blandford & Payne 1982; Camenzind 1990). Submillimeter Array (SMA)[6] observations of linearly polarized dust continuum emission toward the low-mass protostar NGC1333 IRAS4 have clearly shown a pinched hour-glass-shaped magnetic field morphology (Girart et al. 2006). The quest for magnetic fields is just as important in high-mass star formation. Recent submillimeter dust polarization observations have revealed similarly shaped magnetic field morphologies near two massive star-forming regions (Girart et al. 2009; Tang et al. 2009). In addition to that, molecular outflows are known to be as ubiquitous in high-mass star formation as in low-mass star formation, and if the launching mechanisms are of a similar nature, magnetic fields have to be present in massive cores as well.

While most previous high spatial resolution magnetic field studies were either based on dust continuum polarization observations or maser studies (e.g., Girart et al. 2009; Vlemmings 2008b), the molecular gas can also show non-maser spectral line polarization signatures due to the Goldreich–Kylafis effect (Goldreich & Kylafis 1981, 1982). Observations of this effect are particularly promising for studying the magnetic field in molecular outflows (Girart et al. 1999; Lai et al. 2003; Cortes et al. 2005, 2008).

We present a combined polarization study of the 880 μm submillimeter continuum and the CO(3–2) emission toward the well-studied massive disk–outflow system IRAS 18089−1732. The luminosity and gas mass of the region at a distance of 3.6 kpc are $10^{4.5}$ $L_\odot$ and 1200 $M_\odot$, respectively (Sridharan et al. 2002; Beuther et al. 2002; Williams et al. 2004). Vlemmings (2008a) derives for this region a line-of-sight magnetic field strength of 8.4 mG from Zeeman splitting measurements of the 6.7 GHz CH_3OH maser line at densities $>10^6$ cm^{-3}. SMA studies revealed a molecular outflow in an approximately north–south direction and rotational signatures in the dense gas perpendicular to the outflow which were confirmed by high-excitation NH_3 observations (Beuther et al. 2005; Beuther & Walsh 2008). Since IRAS 18089−1732 remains a single compact source up to the highest angular resolution ($<1''$), and since the outflow–disk orientation is well constrained, this region is the ideal target for magnetic field investigation in high-mass star formation.

2. OBSERVATIONS

The region was observed with the SMA in compact and extended configurations in 2008 May and 2009 August. The phase center was R.A. 18:11:51.4, decl. −17:31:28.5 (J2000.0), and the tuning frequency was 345.796 GHz in the upper sideband ($v_{\rm lsr}$ = 33.8 km s^{-1}). While the compact array observations were still conducted in the old setup with 2 GHz bandwidth in both sidebands, the extended configuration data profited from the increased bandwidth of 4 GHz in both sidebands. The spectral resolution in both cases was 0.8125 kHz (∼0.7 km s^{-1}). The weather was good with zenith opacities mostly below 0.25 at 346 GHz. Calibration and imaging were conducted in MIRIAD (Sault et al. 1995). The passband calibration was derived from 3c454.3, and fluxes were calibrated via the regularly monitored SMA calibrator database. The flux density scale is estimated to be accurate within 15%. For the phase and amplitude calibration, regularly interleaved observations of the quasar 1733−130 were conducted. The polarimeter system of the SMA is described in detail in Marrone et al. (2006) and Marrone & Rao (2008). We used 3c273 and 3c454.3 as the polarization calibrator for the compact and extended configuration, respectively. For the

[6] The SMA is a joint project between the Smithsonian Astrophysical Observatory and the Academia Sinica Institute of Astronomy and Astrophysics and is funded by the Smithsonian Institution and the Academia Sinica.

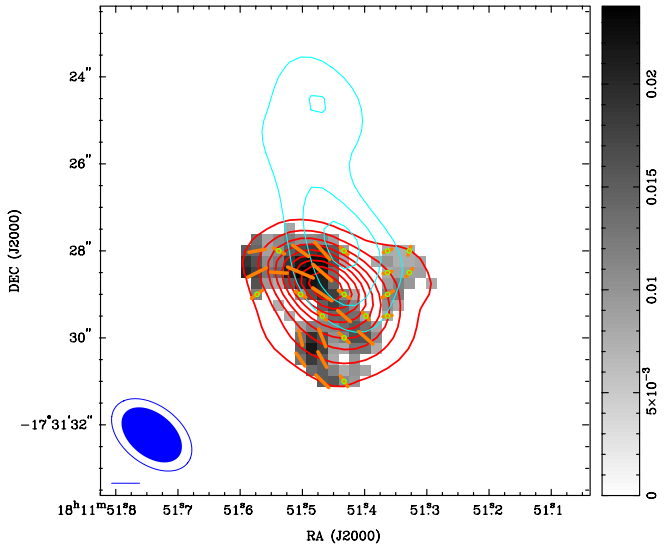

Figure 1. Gray scale presents the linearly polarized 880 μm continuum image of IRAS 18089−1732 in units of Jy beam^{-1}. The line segments plotted in approximate half-beam spacing of 0.″5 show the magnetic field orientation assuming that it is oriented perpendicular to the polarization (line-segment length scales with strength of polarized emission). Line segments marked by a small green circle are those where a 2σ cutoff was applied. The red contours present the integrated Stokes *I* image of the continuum emission in 10σ steps. To outline the outflow direction, the blue contours show the SiO(8–7) emission integrated from 30 to 40 km s^{-1} (5σ steps of 260 mJy beam^{-1}). Full and open ellipses present the synthesized beams of the continuum and SiO emission.

Table 1
Polarization Measurements with Respect to 0/0 Position R.A. (J2000.0) 18:11:51.40 Decl. (J2000.0) −17:31:28.5

Offset (″)	*p* (%)	ϕ (deg)
Dust emission		
1.00,−2.25	5.6	−48
1.50,−1.75	4.2	−66
1.00,−1.75	3.7	−68
0.00,−1.75	2.5	−47
0.50,−1.25	1.4	−42
0.00,−1.25	1.6	−43
1.00,−0.75	1.0	−35
0.50,−0.75	1.0	−38
2.50,−0.25	5.7	33
1.50,−0.25	1.4	−24
1.00,−0.25	1.1	−36
2.50,0.25	4.7	20
2.00,0.25	1.6	−12
1.50,0.25	1.7	−27
1.00,0.25	1.7	−45
2.50,0.75	6.1	1
CO(3–2) at 40 km s^{-1}		
2.00,−12.25	8	−30
0.50,−12.25	8	37
...		

(This table is available in its entirety in a machine-readable form in the online journal. A portion is shown here for guidance regarding its form and content.)

CO(3−2) polarization calibration, we took only the emission from the seven chunks of the bandpass around the CO(3–2) line (approximately 700 MHz). For the continuum data, we used both configurations resulting in a synthesized beam of 1.″65 × 1.″05 (P.A. 51°). Since the CO(3–2) emission is more extended, we used only data from the compact configuration resulting in a synthesized beam of 2.″11 × 1.″34 (P.A. 52°). The 1σ rms values of the continuum Stokes *I* and Stokes *Q*/*U* images are 18.4 mJy beam^{-1} and 4.3 mJy beam^{-1}, respectively, because the noise is dominated by side lobes from strong sources due to insufficient uv-sampling. For the CO(3–2) emission, the 1σ values at 4 km s^{-1} spectral resolution of the Stokes *I* and Stokes *Q*/*U* images are 140 mJy beam^{-1} and 75 mJy beam^{-1}, respectively. The polarized continuum and CO(3–2) images were produced applying a 3σ cutoff to the data. For comparison, for the continuum we also show the results applying 2σ cutoffs in Figure 1. From the other spectral lines in the setup, here we only present the integrated SiO(8–7) emission (Figure 1) to outline the direction of the outflow/jet. The synthesized beam and the rms of the SiO(8–7) image integrated from 30 to 40 km s^{-1} are 2.″11 × 1.″33 (P.A. 52°) and 52 mJy beam^{-1}, respectively.

3. RESULTS

3.1. Submillimeter Dust Continuum Polarization

Figure 1 presents the linearly polarized ($\sqrt{Q^2+U^2}$) as well as Stokes *I* 880 μm continuum emission toward the outflow/disk system IRAS 18089−1732. While the Stokes *I* image exhibits the same single-peaked structure as known from previous observations (e.g., Beuther et al. 2005), the linearly polarized emission has substructure offset from the main peak. The strongest linearly polarized emission with a peak flux of 23.9 mJy beam^{-1} is ∼0.″7 N–NE of the Stokes *I* peak, and the polarized emission shows additional substructure south of the Stokes *I* peak position. At the linearly polarized peak position (R.A. (J2000.0) 18:11:51.51, decl. (J2000.0) −17:31:28.5), the polarization fraction is at an ∼1.5% level, at the Stokes *I* peak position (R.A. (J2000.0) 18:11:51.47, decl. (J2000.0) −17:31:28.8), the polarization fraction is still at an ∼1.1% level (Table 1). The Stokes *I* peak and integrated fluxes within the 10σ contours are 1.93 mJy beam^{-1} and 4.24 Jy, at 880 μm wavelength, respectively. Following Hildebrand (1983), assuming optically thin dust continuum emission with a dust emissivity index $\beta = 2$ at a temperature of ∼100 K (e.g., Beuther et al. 2004) and a gas-to-dust ratio of 186 (e.g., Draine et al. 2007), the derived gas column densities *N* and masses *M* are 9.5×10^{24} cm^{-2} and 197 $M_\odot$, respectively. Taking into account that in particular the mass is a lower limit due to the interferometric missing flux, clearly we are dealing with a high column density and massive core. Assuming a spherical distribution with an approximate core diameter of 3.″5 (linear size of ∼126,00 AU), we get an approximate average core density *n* of 5×10^7 cm^{-3}.

For elliptical dust grains, the polarization orientation of the radiation field is expected to be perpendicular to the magnetic field if the dust grains spin fast enough. Therefore, to infer information about the magnetic field structure, we rotated the line-segment orientation of the polarized emission in Figure 1 by 90° (line segments are shown in approximate Nyquist sampling of 0.″5, indicating the number of independent measurements). In this picture, the overall orientation of the magnetic field component in the plane of the sky follows approximately the general morphological structure of the polarized emission with an orientation roughly along an axis in N–NE to S–SW direction. This general orientation is approximately aligned

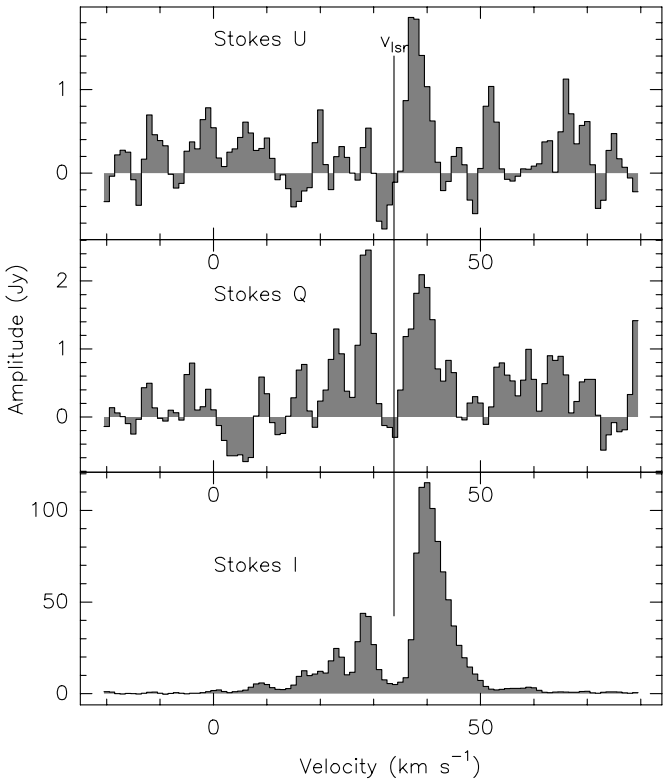

Figure 2. Three panels present vector-averaged spectra of the CO(3–2) line taken on the shortest baseline of the Stokes *I*, *Q*, and *U* components. The vertical line marks the v_{lsr}.

with the outflow traced by the SiO(8–7) emission (Figure 1 and Beuther et al. 2004). Toward the western edge of the core, the field orientation bends a little bit toward the mid-plane of the underlying accretion disk (Beuther & Walsh 2008).

3.2. Polarization of the CO(3–2) Outflow Emission

Furthermore, we observed simultaneously the polarized emission of CO(3−2). Figure 2 presents the Stokes *I* and the linearly polarized Stokes *U* and *Q* spectra obtained vector averaged on the shortest baseline. While the emission at the v_{lsr} is filtered out in all cases, the velocity component around 40 km s^{-1} is not only detected in Stokes *I* but also in both linearly polarized components of Stokes *U* and *Q*. From these data, we derive spatially and spectrally resolved images of the total linearly polarized CO(3–2) emission in this region ($\sqrt{Q^2+U^2}$). Figure 3 shows two 4 km s^{-1} wide channels of polarized CO(3–2) emission around the velocity of 40 km s^{-1}. We again clearly identify the overall N–NE to S–SW outflow direction, but here there is not only the northern component but also a southern counterpart. Since we do not identify a clear blue–redshifted dichotomy, the outflow is likely close to the plane of the sky. The orientation of the polarization follows mainly the outflow direction, and we find polarization degrees in the images of the order of 10% (Table 1), higher than found toward other regions (e.g., Cortes et al. 2005).

3.3. Magnetic Field Strength

Although magnetic field estimates based on polarization data are relatively unreliable since they are based on a statistical analysis of the polarization line segments, nevertheless, we have enough independent polarization measurements in the continuum and line emission that at least rough estimates are useful.

Dust continuum polarization. Following the work by Chandrasekhar & Fermi (1953) and more recently by Girart

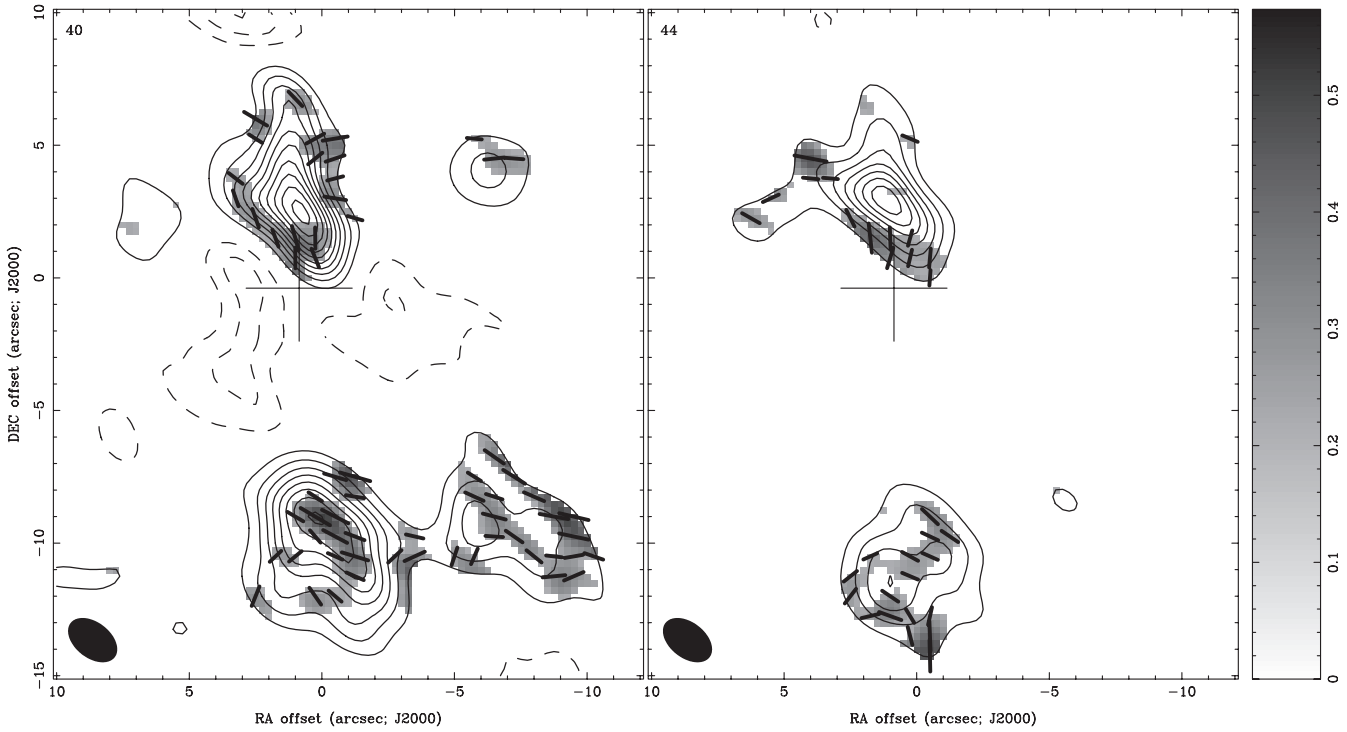

Figure 3. Gray scale presents the linearly polarized CO(3–2) emission in two 4 km s^{-1} wide channels in units of Jy beam^{-1} (central velocities are marked in the top left corners). The line segments plotted in approximate half-beam spacing of 0.″75 show the orientation of the polarized emission (line-segment length scales with strength). The contours present the corresponding CO(3–2) Stokes *I* image in 10σ steps (positive and negative features as full and dashed contours). The cross marks the position of the submm continuum peak. The synthesized beam is shown at the bottom left of each panel.

et al. (2006), we estimate the strength of the magnetic field component in the plane of the sky $B_{\rm pos} \approx Q\sqrt{4\pi\rho}\frac{\Delta v_{\rm los}}{\Delta\phi}$ with ρ the average density derived above in g cm^{-3}, $\Delta v_{\rm los}$ the approximate one-dimensional (1D) velocity dispersion along the line of sight ($\Delta v_{\rm los} \sim \Delta v({\rm CH_3CN})/\sqrt{8\ln 2} \sim 2.2$ km s^{-1} with $\Delta v({\rm CH_3CN}) \sim 5.1$ km s^{-1}; Beuther et al. 2005), and $\Delta\phi$ the approximate flux-weighted dispersion of the polarization angle line segments of $\sim$27°. In practice, we use the rms of flux-weighted line segments ignoring any bending of the field lines which implies that the inferred B-values should be lower limits. Q is a dimensionless parameter accounting for the cloud structure, and work by Ostriker et al. (2001) suggests $Q \sim 0.5$ for turbulent clouds. Since the density ρ depends on the distance d, and the latter is the relatively uncertain kinematic distance, one should keep in mind an additional B-dependence of $B \propto 1/\sqrt{d/3.6\ {\rm kpc}}$. The derived magnetic field strength in the plane of the sky is $B_{\rm pos} \approx 11$ mG. Because Vlemmings (2008a) derives a comparable line-of-sight magnetic field strength for similar densities of the gas from maser Zeeman observations ($B_{\rm los} \approx 8$ mG), the total magnetic field strength at the given core density should be $B_{\rm tot} \approx \sqrt{B_{\rm pos}^2 + B_{\rm los}^2} \approx 14$ mG.

While this is larger than the value previously derived in DR21 (1 mG, albeit measured at a density more than an order of magnitude lower; Lai et al. 2003), it is of the same order as the recent estimates based on dust polarization measurements for G31.41 (Girart et al. 2009) and those derived from CH_3OH maser Zeeman measurements toward a sample of high-mass star-forming regions by Vlemmings (2008a), Vlemmings et al. (2010), and Surcis et al. (2009). The corresponding Alfvénic velocity is $v_A \propto B/\sqrt{\rho} \approx 3.1$ km s^{-1}. The important mass-to-flux ratio can be estimated via $M/\Phi_B \approx 7.6\times10^{-24}\frac{N({\rm H_2})}{B} \approx 5.2$ in units of the critical mass-to-flux ratio $(M/\Phi_B)_{\rm crit}$ ($N({\rm H_2})$ and B are given in cm^{-1} and mG; Crutcher 1999; Troland & Crutcher 2008). While the latter estimate indicates that the magnetic field cannot prevent the core from collapse, comparison of the Alfvénic velocity with the 1D velocity dispersion suggests that the collapse proceeds at approximately or slightly below the Alfvénic speed. Furthermore following Girart et al. (2009), we estimate the ratio of turbulent to magnetic energy via $\beta \approx 3(\Delta v_{\rm los}/v_{A_{\rm los}})^2 \approx 2.5$ (with $v_{A_{\rm los}} \approx 2.4$ km s^{-1} the Alfvénic velocity along the line of sight). Because the estimated $B_{\rm pos}$ is a lower limit, the ratios M/Φ_B and β are upper limits. While for G31.4, W75N, W51, and CepA the magnetic field may play a dominant role determining the dynamics of the systems (Girart et al. 2009; Surcis et al. 2009; Tang et al. 2009; Vlemmings et al. 2010), for IRAS 18089−1732 the system appears to be more strongly dominated by turbulent motions.

CO(3–2) polarization. Following the same Chandrasekhar–Fermi approach as above, we derive a very rough estimate of the magnetic field strength within the outflow lobes. The rms of the polarization angle distribution in the northern lobe is $\Delta\phi \sim 45°$ (again measured as the rms of flux-weighted line segments ignoring any bending of the field lines). However, getting a density estimate based on the given data is far more difficult. Since we cannot derive the density ourselves, we can only assume an average density in the more diffuse envelope where the outflow is observed. Average densities of order 10^3 cm^{-3} should approximately represent the envelope/outflow. With these values and the same line width as for the core, we get magnetic field estimates of order $\sim$28 μG, about three orders of magnitude below the central core magnetic field values. While the Chandrasekhar–Fermi method in principle is prone to many uncertainties—e.g., the $\Delta\phi$ requires subtraction of the ordered magnetic field—it may even be less applicable in the case of the outflow lobes since the outflow may determine most of the polarization orientation. Furthermore, the density uncertainties add to the total uncertainty of the magnetic field estimate. While we cannot give a reliable estimate of this total uncertainty, it is nevertheless likely below three orders of magnitude. Hence, the magnetic field strength in the outflow region appears lower than in the core region. This is consistent with previous results for DR21, where the CO polarization traces magnetic fields of the order 10 μG in the envelope and the dust polarization field strengths of the order mG in the denser core regions (Cortes et al. 2005; Lai et al. 2003).

4. DISCUSSION AND CONCLUSION

The combined polarization data of the submillimeter continuum and the CO(3–2) emission allow us to study the magnetic field structure in the core and outflow of the high-mass disk–outflow system IRAS 18089−1732. For the dust continuum emission, compared to magnetic field hour-glass-shaped structures like those found in NGC1333 or G31.41 (Girart et al. 2006, 2009), the case is less clear here. Inferring an hour-glass-shaped structure indicative of ambipolar diffusion from these data would likely be an overinterpretation. However, in a broader sense this may not be such a surprise. Already Mouschovias & Paleologou (1979) pointed out that adding rotation to the collapsing core could destroy the hour-glass-shaped structure. Therefore, in a statistical sense it may be that finding the hour-glass signatures could be more the exception than the rule. An analysis of a larger sample of sources is required to confirm or reject this hypothesis. Nevertheless, the data of IRAS 18089−1732 are consistent with a picture where the outflow and magnetic field orientation are tightly linked.

For the CO(3–2) emission, since the Goldreich–Kylafis effect occurs only when the line emission is dominated by radiative excitation and not collisions, it sensitively depends on the anisotropy of the optical depth and the radiation field as well as on the orientation of the magnetic field (for a qualitative descriptions see Kylafis 1983). Additionally, an ambiguity exists concerning whether the polarization orientation is perpendicular to or parallel to the magnetic field. However, Cortes et al. (2005) have shown that a large radiation and optical depth anisotropy produces high degrees of polarization parallel to the magnetic field (their Figure 7). Since we observe such a high polarization degree of order 10%, and since the radiation and velocity field is dominated by an anisotropic outflow cone with a central protostellar radiation source, this scenario supports an interpretation that the magnetic field and CO(3–2) polarization orientation in IRAS 18089−1732 are spatially aligned. This is consistent with previous CO polarization studies in DR21 and NGC1333 (Girart et al. 1999; Lai et al. 2003) as well as with the picture of magnetic field accelerated and collimated jets where the magnetic field and outflow should have the same orientation.

To the authors' knowledge, this is the first successful detection of the Goldreich–Kylafis effect in the CO(3–2) line. Comparing the outflow morphology with the polarization direction, it is likely that the magnetic field and polarization both are aligned with the outflow. Although the Chandrasekhar–Fermi method allows only rough magnetic field strength estimates, the data are indicative of a magnetic field strength increase from the envelope toward the core. Furthermore, the observations indicate that turbulent energy likely dominates over magnetic energy.

W.V. acknowledges support by the Deutsche Forschungsgemeinschaft through the Emmy Noether Research grant VL 61/3-1.

REFERENCES

Beuther, H., & Walsh, A. J. 2008, ApJ, 673, L55
Beuther, H., Zhang, Q., Sridharan, T. K., & Chen, Y. 2005, ApJ, 628, 800
Beuther, H., et al. 2002, ApJ, 566, 945
Beuther, H., et al. 2004, ApJ, 616, L23
Blandford, R. D., & Payne, D. G. 1982, MNRAS, 199, 883
Camenzind, M. 1990, in Reviews in Modern Astronomy, Vol. 3, ed. G. Klare, 234
Chandrasekhar, S., & Fermi, E. 1953, ApJ, 118, 113
Cortes, P. C., Crutcher, R. M., Shepherd, D. S., & Bronfman, L. 2008, ApJ, 676, 464
Cortes, P. C., Crutcher, R. M., & Watson, W. D. 2005, ApJ, 628, 780
Crutcher, R. M. 1999, ApJ, 520, 706
Crutcher, R. M. 2005, in IAU Symp. 227, Massive Star Birth: A Crossroads of Astrophysics, ed. R. Cesaroni et al. (Cambridge: Cambridge Univ. Press), 98
Draine, B. T., et al. 2007, ApJ, 663, 866
Girart, J. M., Beltrán, M. T., Zhang, Q., Rao, R., & Estalella, R. 2009, Science, 324, 1408
Girart, J. M., Crutcher, R. M., & Rao, R. 1999, ApJ, 525, L109
Girart, J. M., Rao, R., & Marrone, D. P. 2006, Science, 313, 812
Goldreich, P., & Kylafis, N. D. 1981, ApJ, 243, L75
Goldreich, P., & Kylafis, N. D. 1982, ApJ, 253, 606
Hildebrand, R. H. 1983, QJRAS, 24, 267
Kylafis, N. D. 1983, ApJ, 275, 135
Lai, S., Girart, J. M., & Crutcher, R. M. 2003, ApJ, 598, 392
Marrone, D. P., Moran, J. M., Zhao, J., & Rao, R. 2006, ApJ, 640, 308
Marrone, D. P., & Rao, R. 2008, Proc. SPIE, 7020, 70202B-8
Mouschovias, T. C., & Paleologou, E. V. 1979, ApJ, 230, 204
Ostriker, E. C., Stone, J. M., & Gammie, C. F. 2001, ApJ, 546, 980
Sault, R. J., Teuben, P. J., & Wright, M. C. H. 1995, in ASP Conf. Ser. 77, Astronomical Data Analysis Software and Systems IV, ed. R. A. Shaw, H. E. Payne, & J. J. E. Hayes (San Francisco, CA: ASP), 433
Sridharan, T. K., Beuther, H., Schilke, P., Menten, K. M., & Wyrowski, F. 2002, ApJ, 566, 931
Stahler, S. W., & Palla, F. 2005, The Formation of Stars (New York: Wiley)
Surcis, G., Vlemmings, W. H. T., Dodson, R., & van Langevelde, H. J. 2009, A&A, 506, 757
Tang, Y., et al. 2009, ApJ, 700, 251
Troland, T. H., & Crutcher, R. M. 2008, ApJ, 680, 457
Vlemmings, W. H. T. 2008a, A&A, 484, 773
Vlemmings, W. H. T. 2008b, in ASP Conf. Ser. 387, Massive Star Formation: Observations Confront Theory, ed. H. Beuther, H. Linz, & T. Henning (San Francisco, CA: ASP), 117
Vlemmings, W. H. T., Surcis, G., Torstensson, K. J. E., & van Langevelde, H. J. 2010, MNRAS, 404, 134
Williams, S. J., Fuller, G. A., & Sridharan, T. K. 2004, A&A, 417, 115